ACS central science

Research Article

Cite This: ACS Cent. Sci. 2019, 5, 1920−1928

http://pubs.acs.org/journal/acscii

Atomic-Scale Identification of the Electrochemical Roughening of Platinum

Leon Jacobse,[†,§] Marcel J. Rost,[‡] and Marc T. M. Koper*[,†]

[†]Leiden Institute of Chemistry, Leiden University, P.O. Box 9502, 2300 RA Leiden, The Netherlands

[‡]Huygens−Kamerlingh Onnes Laboratory, Leiden University, P.O. Box 9504, 2300 RA Leiden, The Netherlands

[§]DESY NanoLab, Deutsches Elektronensynchrotron DESY, Notkestrasse 85, D-22607 Hamburg, Germany

Supporting Information

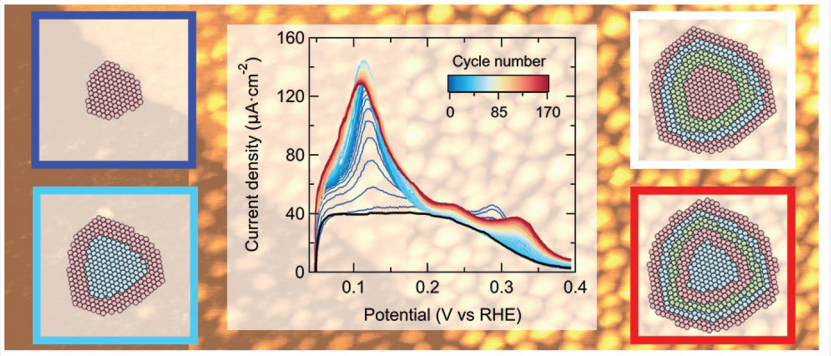

ABSTRACT: Electrode degradation under oxidizing conditions is a major drawback for large-scale applications of platinum electrocatalysts. Subjecting Pt(111) to oxidation−reduction cycles is known to lead to the growth of nanoislands. We study this phenomenon using a combination of simultaneous *in situ* electrochemical scanning tunneling microscopy and cyclic voltammetry. Here, we present a detailed analysis of the formed islands, deriving the (evolution of the) average island growth shape. From the island shapes, we determine the densities of atomic-scale defect sites, e.g., steps and facets, which show an excellent correlation with the different voltammetric hydrogen adsorption peaks. Based on this combination of electrochemical scanning tunneling microscopy (EC-STM) and CV data, we derive a detailed atomistic picture of the nanoisland evolution during potential cycling, delivering new insights into the initial stages of platinum electrode degradation.

INTRODUCTION

Subjecting a platinum electrode to oxidation−reduction cycles (ORCs) is one of the most commonly performed experiments in surface electrochemistry. This pretreatment cleans the platinum surface and results in a reproducible (albeit typically unknown) surface structure.[1−3] It is well-known that the Pt surface undergoes a significant structural transformation during this process, as is most dramatically illustrated when starting with a well-defined Pt(111) single crystal electrode.[4] Understanding the roughening of a Pt(111) electrode by ORCs at the atomic scale has therefore been a long-standing goal in fundamental electrochemistry.

A fingerprint of the average surface structure of platinum electrodes can be obtained with voltammetric experiments, as the adsorption and desorption of hydrogen are very sensitive to the atomic-scale surface sites available for this reaction. Especially for low-index single-crystal surfaces, these hydrogen adsorption features and their evolution upon potential cycling have been studied extensively.[5−8] Complementary information from vicinal surfaces has resulted in a qualitative description of the roughness formation on Pt(111) by the generation of mainly {100} surface sites first, followed by the generation of {111} surface sites. To quantify this process, Björling et al. constructed a kinetic model, describing the evolution of the hydrogen features during the first 20 ORCs.[9,10] However, without direct, *in situ* spatial information, data from cyclic voltammetry (CV) alone have been insufficient to describe (the evolution of) the surface structure at the atomic scale.[4,9,10]

Spatially resolved data are available from *ex situ* low-energy electron diffraction (LEED),[11,12] *in situ* X-ray reflectivity,[13−20] and *in situ* electrochemical scanning tunneling microscopy (EC-STM)[21−27] experiments. For a brief recent review, see the paper by Drnec et al.[28] From these data, it is known that applying ORCs to a Pt(111) electrode leads to the growth of small (typically ∼8 nm) nanoislands on the surface. However, a detailed structural characterization as well as a full electrochemical characterization (measured in the same experiment) are still missing. As such, the complex evolution of the electrochemical fingerprint signal has as of yet remained unexplained. By combining *in situ* EC-STM with CVs in a single experiment, we have recently demonstrated that the

Received: August 3, 2019
Published: November 15, 2019

growth of nanoscale islands, and therefore the electrode roughness, is directly correlated to the integrated hydrogen desorption in the voltammetric signal.[29] This integrated correlation, however, is "blind" to the different contributions from individual local surface geometries/sites. Nonetheless, the EC-STM data as well as the CVs do contain this detailed information on the individual local sites. We extract this information by applying a careful analysis to both the individual CVs and the average growth shapes of the nanoscale islands.

In this Article, we disentangle the hydrogen desorption region of the CVs into the individual site specific peaks to quantify the different "defect-related" contributions. From the EC-STM images measured in the same experiment, we extract the average nanoisland growth shape as a function of the number of applied ORCs. These shapes contain the densities of specific undercoordinated ("defect") sites, i.e., steps, facets, and kinks on the roughened Pt(111) surface. The combined measurements enable us to correlate the CVs with the EC-STM data, made possible by employing a home-built EC-STM described previously.[30−32] Based on this combination, we can draw a detailed atomic-scale picture of the nanoisland evolution during ORCs. This picture describes the initial stages of the electrochemical roughening of platinum and provides insight for the understanding of the degradation of Pt catalysts under dynamic operation.

RESULTS AND DISCUSSION

Electrochemical Measurements. The desorption of underpotential deposited hydrogen (H_{UPD}, $0 < U_s < 0.4$ V) contains detailed information on the average atomic surface structure of the electrode under consideration. For Pt(111) in 0.1 M $HClO_4$, this region shows only a very broad, flat feature related to hydrogen desorption from atomically smooth (111) terraces, as indicated by the black line in Figure 1A. From this

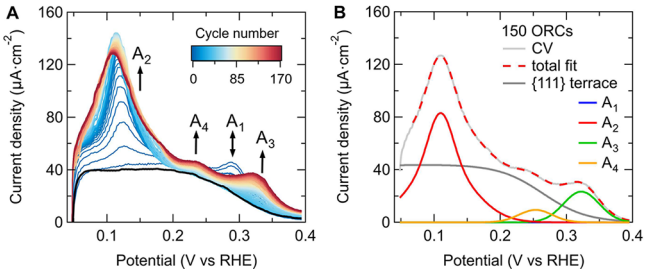

Figure 1. Evolution of the electrochemical fingerprint upon surface roughening. (A) H_{UPD} region of the 170 subsequent (from blue to red) oxidation−reduction cycles between 0.06 and 1.35 V. The CV of the initial, well-prepared Pt(111) surface is shown in black. Four "defect-related" peaks, labeled A_{1-4}, are observed during the overall process. The potential scan rate is 50 mV s^{-1}, and the electrolyte is 0.1 M $HClO_4$. (B) Example of the fit result to determine the individual peak charges for the situation after 150 ORCs.

starting situation, the sample potential is cycled between 0.06 and 1.35 V (with 50 mV s^{-1}), leading to the growth of nanoislands as shown previously.[19,21−27,29] Simultaneously to this roughening process the electrochemical fingerprint changes drastically as shown in Figure 1A. The appearance of four distinct new peaks, labeled A_{1-4}, indicates the formation of new "defects" (specific local atomic sites in the nanoislands).

To enable a correlation of the CV features with specific surface site densities, we have to disentangle the charge corresponding to these four H_{UPD} peaks. Several approaches have been presented in the literature, for both single crystalline and nanoparticle samples.[33−36] However, especially for very rough surfaces, deconvoluting the H_{UPD} region shows some discrepancy with results from other electrochemical experiments.[33,35] One of the underlying reasons is that the broad (111) terrace feature (black line in Figure 1A) changes its shape for more narrow terraces and overlaps with all four "defect" peaks.[37] Thus, the terrace feature is typically considered to be a background signal.[10] In our fitting procedure, we therefore also follow this approach by keeping the terrace contribution constant for all cycles. As the number of terrace sites is expected to decrease during the surface roughening, we most likely underestimate the charge related to H_{UPD} at "defects". Following McCrum and Janik, the broad terrace feature is fitted with an inverse hyperbolic cosine function, and the A_{1-4} peaks are fitted with Gaussians.[35] To capture the changing shape of the A_2 peak, it is necessary to use a summation of two Gaussians. Most consistent fit results were obtained by centering these two Gaussians at the same potential. An example of the fitting result, for the situation after 150 ORCs, is shown in Figure 1B.

Figure 2A shows the integrated charges of the A_{1-4} peaks in the CVs as a function of the number of applied ORCs. The overall process can be separated in different regimes: both the A_1 and A_2 peaks increase during the first few ORCs; already

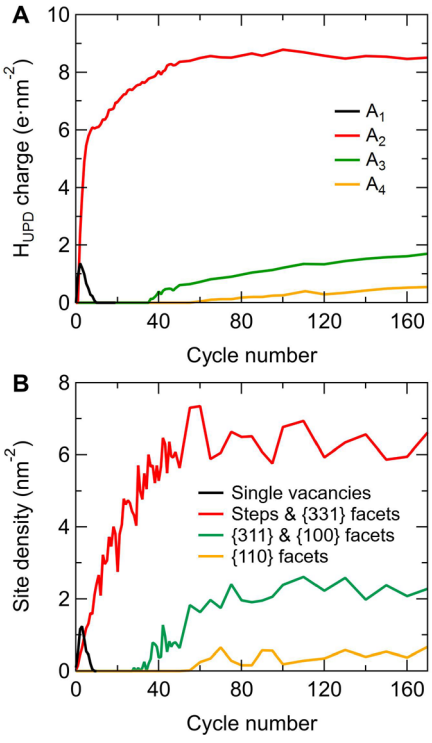

Figure 2. Evolution of peak charges and corresponding adsorption site densities. (A) Integrated charges of the A_{1-4} peaks in the H_{UPD} region shown in Figure 1A. (B) Densities of single vacancies, step sites + {331} facets, {311} + {100} facets, and {110} facets as counted from the average atomic-scale island shapes in Figure 3B. Note that {221} and {211} facets (blue in Figure 4) are counted as "separated steps" (see the main text). Further motivations behind grouping (correlating) the various sites are provided in the main text.

DOI: 10.1021/acscentsci.9b00782
ACS Cent. Sci. 2019, 5, 1920−1928

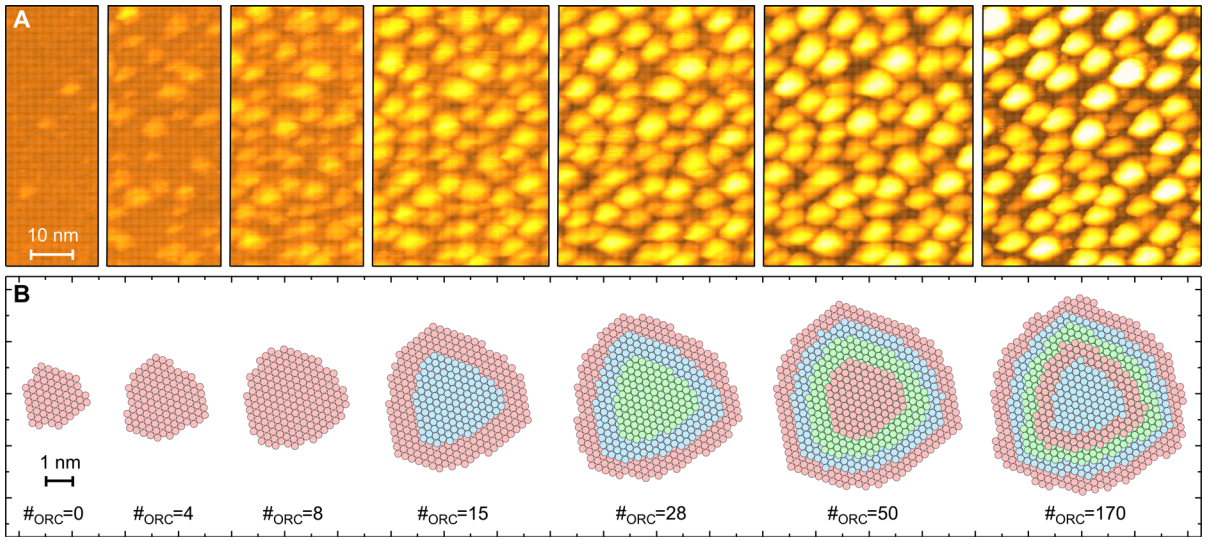

Figure 3. EC-STM images and average nanoisland structures. (A) Parts of EC-STM images after 0, 4, 8, 15, 28, 50, and 170 ORCs (from left to right) illustrating the roughening of a single surface area. The original, individual images are 230 × 230 nm^2, recorded with U_{tip} = 0.45 V, U_{sample} = 0.4 V, and $I_{tunneling}$ < 300 pA. Note that the total contrast is the same for the different images. The full set of EC-STM images is available in ref 29. (B) Average atomic-scale growth structure of the islands as determined from the EC-STM images for the same situations as shown in part A. The different colors indicate the different atomic layers in the island. The full image sequence is provided in the Supporting Information.

after two ORCs A_1 starts to decrease, and it has disappeared after 10 ORCs, while A_2 keeps increasing continuously. This is in agreement with the original observations in refs 9 and 10. After further cycling, the A_3 and A_4 peaks appear after 36 and 60 ORCs, respectively. In the literature, the A_1 and A_2 peaks (and their evolution) have been ascribed to the presence of {100} and {111} steps at the surface, respectively.[4,9,10] It is expected that steps form during the roughening of an atomically flat surface. However, the relative charges of the A_1 and A_2 peak are puzzling. Based on its peak potential, one expects the A_3 peak to be related to the formation of {100} terraces.[38,39] The A_4 peak is also known as "the third hydrogen peak".[40,41] Although the exact origin of this peak is heavily debated, it is suggested to be related to the presence of (1 × 2) {110} sites at the surface.[40] Especially for the latter two peaks, it is not clear how these expected "defects" are formed on the roughened surface. Finally, it is important to stress that the changing shape and peak potential of the A_2 peak upon prolonged potential cycling indicate that this peak actually consists of more than one contribution. In the following, we will see how the evolution of the individual surface sites as a function of number of applied ORCs (Figure 2A) correlates with the atomic sites extracted from the average island growth shape.

Average Growth Shape Determination. Next, we discuss the determination of surface site densities extracted from the average island shapes from the EC-STM images. The result of this analysis is already shown in Figure 2B for comparison with the evolution of the electrochemical fingerprint shown in Figure 2A.

Figure 3A shows clippings of the EC-STM images after 0, 4, 8, 15, 28, 50, and 170 ORCs. These clippings have been selected from the full set of 230 × 230 nm^2 images, which have been measured with constant tip and sample potential (0.45 and 0.4 V, respectively).[29] With a resolution of 2.25 Å pixel^{-1}, our images are not directly atomically resolved. In addition, considering the surface roughness and tip convolution, achieving full atomic resolution would be extremely challenging. Nonetheless, the average atomic-scale island shape representative for a certain number of ORCs can be determined by a careful data analysis, described in detail in the Supporting Information. In brief, the images are corrected for drift and height offset; approximate island centers are determined by threshold and watershed functions, and island boundaries are determined by a combination of Laplace filtering and the construction of Voronoi cells. In the next step, we average all height profiles of the individual islands present in one EC-STM image, by taking the local maximum as island center. Finally, the average island shape is fitted with an fcc lattice, taking into account the main step directions on the surface. From repeated experiments (see the Supporting Information) we argue that the shapes of the islands on our wide terraces are not affected by the step edges present in the pristine surface. Thus, any asymmetry deviating from the 3-fold symmetry of the Pt(111) surface originates from the shape of the STM tip. To minimize this imaging artifact, the fitting procedure imposes a 3-fold island symmetry.

Previously, we have shown that the area visualized in our EC-STM images is large enough to describe the roughening of the entire Pt(111) surface.[29] Except for the first cycles, when the island density is rather low, the analyzed areas typically contain between 400 and 500 individual islands. Because of the large number of averaged islands, the resulting island structure is considered to be representative of the statistical growth shape after a certain number of ORCs.[42] It is important to note that such growth shapes differ from classical Wulff shapes in thermodynamic equilibrium.[42] Finally, one could argue that the hydrogen desorption features result from the integrated rather than the average surface structure. However, as the growth shapes are rather homogeneous, this difference is not expected to lead to significant differences in the analysis.

Figure 3B shows the results of the fitting procedure applied to the *full* EC-STM images after 0, 4, 8, 15, 28, 50, and 170 ORCs, i.e., those that are partly shown in Figure 3A. The full series of island structures is provided as a movie in the Supporting Information.

DOI: 10.1021/acscentsci.9b00782
ACS Cent. Sci. 2019, 5, 1920−1928

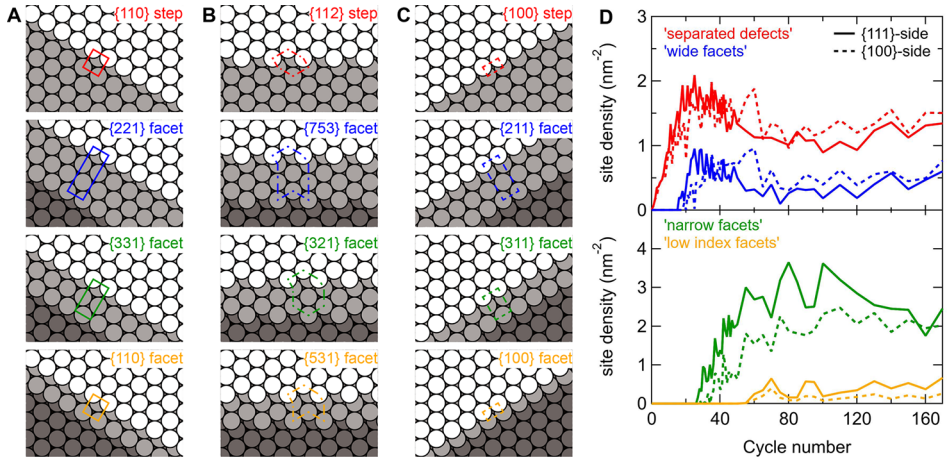

Figure 4. Unit cells and time evolution of "defect" site densities derived from average nanoisland structures. (A−C) Representative unit cells for the {111}-, {112}-, and {100}-side steps/facets, respectively. The structures range from "separated steps" (top) to "low-index facets" (bottom). All counting rules and unit cells for other possible structures, as well as all individual site densities, are provided in the Supporting Information. (D) Site densities for the "separated steps" and "wide facets" (top), and "narrow facets" and "low-index facets" (bottom) for both the {111}- and {100}-side (solid and dashed lines, respectively).

Determination of "Defect" Site Densities. From the atomic island structures it is possible to determine the densities of the different atomic sites at the surface. Detailed descriptions and counting rules for the various sites are explained in the Supporting Information. Here, we provide the general considerations. Due to the symmetry of the Pt(111) surface, we distinguish three different directions in the surface plane as shown in Figure 4A−C. In the following, we will refer to these directions according to the step site geometry at the corresponding side of the island: {111} steps are found at the {111}-side (Figure 4A) and {100} steps at the {100}-side (Figure 4C). Step edges in the third direction (Figure 4B are oriented at midangle between these two densely packed directions. They have a {112} geometry and are typically described as "100% kinked".[43] Note that these {112} sites have a distinct geometry, which cannot be constructed by the formation of kink sites in a {100} or {111} step edge. However, the literature data for surfaces containing these step sites (only available for Pt(321) and Pt(531)[44]) indicate that the presence of {112} step edges does not lead to an additional specific feature. Instead, two peaks are observed, which overlap with the peaks related to {100} and {111} steps. The same is observed for surfaces containing kinked {100} or {111} step edges.[44,45] Furthermore, the densities of {112}-related sites and kink sites exhibit large variations between subsequent ORCs. This is expected to be a fitting artifact. In our analysis, we will, therefore, distribute these sites according to the two main island sides (i.e., the {111}- and {100}-side). More details on the grouping are given in the Supporting Information.

Apart from the geometry, the spacing between "defects" (steps) in the different layers is known to have a significant effect on their electrochemical reactivity.[37] Step edges separated by less than two terrace atoms (as on the (221) and (211) surfaces) bind hydrogen stronger than wider spaced step edges, as indicated by a more positive peak potential. To capture this effect, we consider the following: (1) step edges separated by more than two terrace atoms ("separated steps", e.g., {110} and {100} steps); (2) step edges separated by two terrace atoms ("wide facets", e.g., {221} and {211} facets); (3) step edges separated by one terrace atom ("narrow facets", e.g., {331} and {311} facets); and (4) adjacent step edges ("low-index facets", e.g., {110} and {100} facets). Unit cells of the steps and facets for the {111}-, {112}-, and {100}-side are shown in Figure 4A−C, respectively. We also take into account that terrace sites that are adjacent to a "defect" site could exhibit a different reactivity. Detailed counting and grouping rules for all sites are provided in the Supporting Information. Finally, we obtain site densities distributed over eight different groups (i.e., the {111}- and {100}-side and the four different terrace spacings). The evolution of these site densities as a function of cycle number is shown in Figure 4D.

Initially, only "separated steps" form, whereas the different kinds of facets only appear after prolonged potential cycling (after 16, 27, and 55 ORCs for "wide", "narrow", and "low-index" facets, respectively). This is in line with the observations in our previous study, where we showed that the nanoislands first nucleate and (mainly) grow laterally, before growing in height.[29] Height growth, with a fixed island base, ultimately leads to the formation of facets. Although the islands are rather symmetric, the formation of facets is initially seen at slightly higher intensity at the {111}-side. This is because the unit cell of a {110} step is longer than that of a {100} step. The number of terrace sites on the island (see the Supporting Information) first increases but starts decreasing when facets are formed in terrace sites. Including also the (original) terrace sites that are not part of the island, a continuous decrease is observed.

Step Edge Formation. We now correlate the evolution of the electrochemical fingerprint (Figure 2A) with the evolution of the "defect" site densities (Figure 4D). We start the discussion with the simplest case. This is the situation between 10 and 30 ORCs, as here the A_2 peak is the only "defect" feature visible in the CV. The absence of the A_1 peak indicates that there are no {100} steps at the surface. Thus, one might expect to observe triangular nanoislands composed of only {111}-sides. However, the images in Figure 3B, e.g., after 15 ORCs, clearly show that this is not the case, as an extended {100}-type step length is present in the average island growth shape. This is quantified in Figure 4D (red dashed line) which also clearly indicates substantial densities of {100} step sites.

The only way to explain the significant step length at the {100}-side of the island without the actual formation of {100}

DOI: 10.1021/acscentsci.9b00782
ACS Cent. Sci. 2019, 5, 1920−1928

step sites is by assuming that these step edges are in reality "roughened"[46] and thereby composed of small segments of {110} steps as illustrated in Figure 5. This hypothesis is

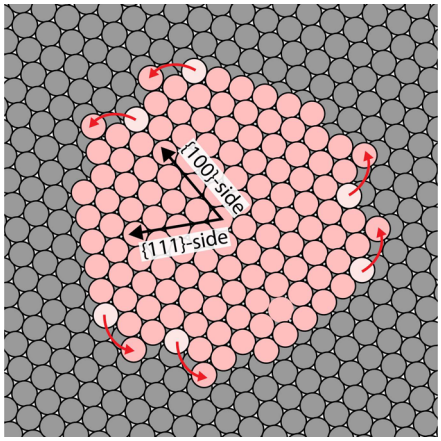

Figure 5. Step "roughening" example: Example of a (mass conserved) step "roughening" to minimize the number of {100} step sites. Such step structures are necessary to explain the island symmetry in combination with the presence of only one "defect" peak in the CVs between 10 and 30 ORCs, see Figure 2.

supported by data from the group of Feliu on the roughening of Pt(11 10 10), a surface which naturally contains {100} steps.[47] These data show that {100} step edges are highly unstable during the ORCs: their voltammetric feature diminishes quickly upon potential cycling (almost completely during the first ORC) and is replaced by a {110} peak.[10] Similar observations were made by Rodes and Clavilier, who studied the electrochemical behavior of various single-crystal surfaces with {100} step edges as a function of annealing/cooling conditions and potential cycling.[7]

The "roughened" hexagonal islands (Figure 5) will only be preferred over triangular islands if the step sites at the {100}-side are stabilized somewhere during potential cycling. This expectation is supported by DFT calculations on low-index Pt surfaces under electrochemical conditions, which likely show the same trend as the step edges.[48] These calculations indicate that Pt(100) is more stable than Pt(110) at high potentials (>0.9 V for the surface oxide and >1.05 V for adsorbed O/OH). At reducing potentials, however, the {110}-facet is more stable, delivering the driving force for the step edge "roughening". Unfortunately, the step edge "roughening" is not captured in our fitting results. The reason for this is both the averaging process for the determination of the average island shape and the limited resolution of our EC-STM images. The study by Rodes and Clavilier has shown that when "separated" step edges are roughened, the increase in charge of the A_2 peak is twice the decrease in charge of the A_1 peak.[7] This is ascribed to the formation of two kink sites from one step site. Thus, in our correlation analysis we argue that each "separated" {100} step site contributes double to the A_2 peak. The facets at the {100}-side and their "roughening", which could also contribute to the A_2 peak, are discussed below.

Vacancies and Vacancy Islands. Considering that the {100} step sites are unstable under ORCs, an alternative explanation is needed for the A_1 peak. Interestingly, there is no surface site in the adatom islands that, after appearing during the first two cycles, disappears completely after 10 ORCs, as suggested by this peak. Importantly, the islands are only one atom high when this peak is present, which excludes a relation to the formation of any kind of facet site. One could imagine that this peak is related to the presence of "separated" {100} step sites which did not yet "roughen", e.g., due to a very small island size. However, if that were true, this peak would reappear once a new layer nucleates on top of an existing island, i.e., after 9, 16, 30, and 55 ORCs. Alternatively, it should not disappear completely, considering that the values for nucleation of a new layer are averages, and in reality there is some heterogeneity between the islands. Furthermore, it is also unlikely that this peak originates from a surface miscut as this cannot explain why it increases during the first cycles, nor why the charge is 2−3 orders of magnitude larger than what would be expected from the step density observed in the EC-STM images. In conclusion, this peak must represent a surface site that is solely present in the very beginning of the entire roughening process and that is not present in the adatom islands.

Previously, we observed that vacancies form simultaneously with the adatom islands.[29] These small vacancies are extremely difficult to resolve in STM and will, especially at low coverages, not contribute to the average island structure. However, the reactivities of terrace sites that are immediately adjacent to a vacancy are affected nonetheless. As the surface roughening is (almost completely) mass conserved, the total number of vacancies (single vacancies and vacancy islands) must be the same as the number of adatoms forming the average island shape.[49−52] This enables us to describe the expected vacancy-related signal. First of all, this signal depends on the number of created adatoms, which determines both the number of vacancy sites and the number of unaffected terrace sites. The number of terrace sites that are actually adjacent to a vacancy site is determined by the possible nucleation of single vacancies into vacancy islands of a specific size (n), as illustrated in Figure 6.

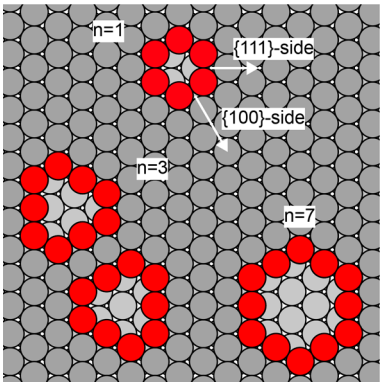

Figure 6. Vacancy site formation. Affected vacancy edge sites (red) for single vacancies and vacancy islands of 3 and 7 atoms (so-called magic clusters[56]). The arrows at the single vacancy indicate the two nonequivalent directions. Note that two different island orientations exist for the n = 3 vacancy island.

We find a very strong correlation between the charge of the A_1 peak (r = 0.96) and the expected vacancy signal (see the Supporting Information), when considering the formation of single, isolated vacancies. This expected signal is shown in black in Figure 2B. As the surface roughening remains almost mass conserved also after a large number of ORCs, further formation of vacancies in underlying surface layers must occur.

DOI: 10.1021/acscentsci.9b00782
ACS Cent. Sci. 2019, 5, 1920−1928

However, due to the increased total surface roughness, adatom and vacancy sites are no longer widely separated. Now, the vacancy sites become part of the islands and are thus captured by our fitting procedure. Most likely, step edge "roughening" is the reason for the absence of the A_1 peak. The evolution of the nano-island growth has been analyzed in detail and an analytic, atomic model has been developed that describes the growth satisfactorily. This delivers insight in the atomic processes taking place and explains exactly how and why these islands are formed.[52] Considering the simplicity of our approach, the level of correlation is remarkable as nucleation of vacancy islands, vacancy formation within vacancy islands, and surface reconstruction[53−55] could occur. In any case, we can conclude that the A_1 peak is related to the formation of vacancy sites in the (111) terrace, although the full explanation will likely be more complex than our simple model.

The peak potential of the A_1 peak suggests that its signal originates only from {100} sites. A step edge description is probably not valid for single vacancies, but according to the symmetry, one would expect another vacancy feature related to {111} sites. With our limited information it is impossible to discern such a contribution, but we do note that, during the first ∼20 cycles, the number of sites contributing to the A_2 peak is underestimated (see Figure 2 and the Supporting Information). The discrepancy is largest during the first three ORCs and then diminishes, which hints at a relationship to the formation of vacancy (island) sites.

Facet Formation. Next, let us consider the A_3 and A_4 peaks, which appear only after prolonged potential cycling. Their "late" appearance indicates that they are related to the formation of specific facets due to the height growth of the nanoislands. This is confirmed when inspecting the average island shape after 28 ORCs in Figure 3B: all standard step and kink sites are present, but the A_3 and A_4 peaks do not yet contribute to the CV.

The charge of the A_3 peak is clearly correlated to the density of {311} facet sites (correlation coefficient r = 0.92, see the Supporting Information). This is in line with the A_3 peak potential (∼0.32 V), which is slightly higher than that of {100} step sites.[37] Interestingly, this correlation must mean that the {311} facet is stable enough to withstand the step edge "roughening", which occurs for the "separated" {100} step sites. Indeed, roughening experiments of Pt(311) by thermal or electrochemical adsorption of oxygen do not show any formation of {110} step/kink sites.[7] The stabilization of straight step edges for narrow terraces can be ascribed to the repulsive interaction between step edges of equal sign[57] and has been observed before for stepped Pt surfaces.[58] Our data also provide some insight in the minimum terrace width necessary to sufficiently stabilize the {100} step sites. As the {211} facets appear 10 cycles before the emergence of the A_3 peak, we conclude that also this facet must roughen. As such, it contributes to the A_2 peak. This result is in line with previous potential cycling experiments,[59] although thermal oxidation experiments indicate that the {211} facet withstands step "roughening".[7] Most likely, the {100} facets contribute as well to the A_3 peak.[37] Indeed, the summation of the densities of {311} and {100} facets (the green line in Figure 2B) leads to a slightly higher correlation coefficient (0.93, see the Supporting Information).

As the A_4 peak appears later than the A_3 peak, it is expected that this peak is related to the formation of facets that are even narrower than the {311} facets. Considering the peak potential, these sites are likely formed at the {111}-side of the islands. Nonetheless, the correlation between the {110} facets (yellow line in Figure 2B) and the A_4 charge is rather low (r = 0.54). Upon closer inspection (see the Supporting Information), it becomes clear that this is mainly due to the large variation in the density of {110} facets between subsequent cycles. After applying a moving average filter (averaging over 5 data points) to the {110} facet density, the correlation coefficient is significantly increased (r = 0.93, see the Supporting Information).

The A_2 peak for the roughened surface is much broader than for a regularly stepped single crystal. This complicates the separate identification of {111}-side facets, as these features overlap in our CVs. This overlap is confirmed by the increase of the correlation coefficient between the A_2 charge and the site densities when the {331} facet sites are included (r = 0.88 vs 0.76). The correlation analysis also indicates that the "wide facets" are better described as "separated steps"; i.e., the adjacent terrace sites do not contribute to the A_2 peak (see the Supporting Information). This suggests that the small facet-related features as observed for Pt(221) and Pt(211) are actually due to the terrace width distribution of these surfaces.[37] The summation of all sites contributing to the A_2 peak (all "separated steps" and the {331} facets) is shown as the red curve in Figure 2B.

Final Remarks. Our analysis shows that site densities extracted from EC-STM images are in good accordance with the evolution of the cyclic voltammetry during the surface roughening. It is interesting to look at the prefactors of these correlations, which have been worked out in detail in the Supporting Information. In the traditional picture of adsorption/desorption of a single hydrogen atom at each "defect" site, one would expect all prefactors to be unity.[5−8] However, recent studies demonstrate that the "defect" features in the H_{UPD} region are actually not just adsorption/desorption of hydrogen, but rather a replacement of hydrogen atoms by hydroxyl groups.[60,61] As a result, the expected transferred charge per surface site should be larger than 1 e^-. Experimental results point in this direction, albeit without quantification, for widely spaced {110} step edges.[62] However, it is not directly clear to what extent these values are affected by the applied fitting procedure. Our prefactors for the A_1 and A_2 peaks (1.07 ± 0.07 and 1.46 ± 0.04 e^-/site, respectively) match these expectations. The prefactors for the A_3 and A_4 peaks (0.56 ± 0.02, and 0.77 ± 0.06 e^-/site, respectively), on the other hand, seem to be too small. This can be explained by our fitting procedure, in which we keep the terrace contribution constant. Single crystal experiments show that the broad (111) terrace feature changes shape, i.e., loses intensity mainly at high potentials, due to the formation of narrow terraces.[37] This leads to an underestimation of the "defect" peaks, in particular the A_3 and A_4 peaks, which appear with narrowing terraces.

Finally, one should be aware of the limitations of counting absolute site densities from the EC-STM images. As it is impossible to fully correct for tip convolution effects, there will always be some uncertainty in the determined densities; the size of the islands will be slightly overestimated, whereas the depth of the "holes" in between the islands is not fully resolved. Another uncertainty comes from the step edge "roughening", which is also not directly resolved. The available literature data for kinked surfaces are not sufficient to rigorously prove that the corner and fully kinked step "defects" contribute equally to the {100}- and {110}-related CV features. This was an

DOI: 10.1021/acscentsci.9b00782
ACS Cent. Sci. 2019, 5, 1920−1928

underlying assumption of grouping the site densities as performed in Figure 4D. Thus, although the current values of our prefactors are in the right range, they should be interpreted with some care.

CONCLUSION

By carefully combining cyclic voltammetry (CV) experiments with *in situ* EC-STM images obtained on the same surface in the same electrochemical cell, we can draw an atomistic picture of how nanoislands form and evolve during the oxidation−reduction cycles (ORCs) of a Pt(111) electrode in perchloric acid solution. A detailed analysis of the overall interlayer mass transport is provided elsewhere.[52] During the first ORCs, the formation of a thin platinum oxide and its subsequent reduction lead to the formation of Pt adatoms and vacancies on the Pt(111) surface. These Pt adatoms nucleate into monatomic height islands. The Pt(111) vacancies give rise to the A_1 peak in the CV, a peak which initially grows but loses intensity after a few cycles as the original Pt(111) surface disappears. The monatomic islands have a dominant 6-fold symmetry but show only a single {111}-type step edge, leading to the A_2 peak in the CV, because the {100} step edges are roughened due their instability under surface oxidation. This latter observation is in good agreement with the oxygen-induced roughening of {100} step edges on model single-crystal electrodes.[10] Upon prolonged cycling, a second layer grows on top of the first adlayer island, and the islands reach a size at which they start touching each other. After this initial phase of nucleation and growth, no new islands form, and existing islands only grow in height.[29] This vertical growth of nanoislands leads to the appearance of two new peaks in the CV, A_3 and A_4, which correspond to {100}- and {110}-type step edges and defects bordering narrow terraces: facets are formed. The {100}-type step edges are now stable because the step edge roughening is suppressed by the strong step−step repulsion related to the narrow terraces.[58] The atomistic description of the roughening of a Pt(111) electrode gives detailed insight into the specific atomic geometries that form during potential cycling experiments in a way that is consistent with both the CV and EC-STM measurements, as well as with previous experiments on model electrodes. These insights form valuable input for the further development of platinum electrocatalysts which exhibit both a high activity and a long lifetime.

ASSOCIATED CONTENT

Supporting Information

The Supporting Information is available free of charge on the ACS Publications website at DOI: 10.1021/acscentsci.9b00782.

Additional experimental details and figures including EC-STM images, distortion correction, 2D autocorrelation analysis, fitting results, site assignment, site densities, and vacancy site formation (PDF)

Movie S1: full set of all 68 uncompressed STM images (MP4)

Movie S2: atomic island structures, resulting from a fitting procedure (MP4)

AUTHOR INFORMATION

Corresponding Author

*E-mail: m.koper@lic.leidenuniv.nl.

ORCID

Leon Jacobse: 0000-0002-2825-0963

Marc T. M. Koper: 0000-0001-6777-4594

Notes

The authors declare no competing financial interest.

ACKNOWLEDGMENTS

This work is part of the research programme TOP with project number 716.017.001, which is financed by The Netherlands Organisation for Scientific Research (NWO). The authors acknowledge LVH Coatings for supplying their Clearclad electrophoretic paint.

REFERENCES

(1) Bard, A. J.; Faulkner, L. R. *Electrochemical Methods: Fundamentals and Applications*, 2nd ed.; John Wiley & Sons, Inc., 2001; p 864.

(2) Schmickler, W., Santos, E. *Interfacial Electrochemistry*; Springer-Verlag: Berlin Heidelberg, 2010; p 272.

(3) Santos, E., Schmickler, W. *Catalysis in Electrochemistry: From Fundamental Aspects to Strategies for Fuel Cell Development*; John Wiley & Sons, Inc., 2011; p 516.

(4) Gómez-Marín, A. M.; Feliu, J. M. Pt(111) Surface Disorder Kinetics in Perchloric Acid Solutions and the Influence of Specific Anion Adsorption. *Electrochim. Acta* **2012**, *82*, 558−569.

(5) Clavilier, J.; El Achi, K.; Rodes, A. In Situ Characterization of the Pt(S)-[n(111) x (111)] Electrode Surfaces using Electrosorbed Hydrogen for Probing Terrace an Step Sites. *J. Electroanal. Chem. Interfacial Electrochem.* **1989**, *272*, 253−261.

(6) Rodes, A.; El Achi, K.; Zamakhchari, M. A.; Clavilier, J. Hydrogen Probing of Step and Terrace Sites on Pt(S)-[n(111) x (100)] Electrodes. *J. Electroanal. Chem. Interfacial Electrochem.* **1990**, *284*, 245−253.

(7) Rodes, A.; Clavilier, J. Electrochemical Study of Step Reconstruction on Platinum Surfaces Belonging to the [011] Zone between Pt(311) and Pt(111). *J. Electroanal. Chem.* **1993**, *344*, 269−288.

(8) Clavilier, J.; Rodes, A. Electrochemical Detection and Characterization at Pt(N,N,N-2) Oriented Electrodes of Multiatomic Step Formation Induced by Quenching at High-Temperatures. *J. Electroanal. Chem.* **1993**, *348*, 247−264.

(9) Björling, A.; Ahlberg, E.; Feliu, J. M. Kinetics of Surface Modification Induced by Submonolayer Electrochemical Oxygen Adsorption on Pt(1 1 1). *Electrochem. Commun.* **2010**, *12*, 359−361.

(10) Björling, A.; Feliu, J. M. Electrochemical Surface Reordering of Pt(111): A Quantification of the Place-exchange Process. *J. Electroanal. Chem.* **2011**, *662*, 17−24.

(11) Wagner, F. T.; Ross, P. N. LEED Spot Profile Analysis of the Structure of Electrochemically Treated Pt(100) and Pt(111) Surfaces. *Surf. Sci.* **1985**, *160*, 305−330.

(12) Aberdam, D.; Durand, R.; Faure, R.; El-Omar, F. Structural Changes of a Pt(111) Electrode Induced by Electrosorption of Oxygen in Acidic Solutions: a Coupled voltammetry, LEED and AES study. *Surf. Sci.* **1986**, *171*, 303−330.

(13) You, H.; Zurawski, D. J.; Nagy, Z.; Yonco, R. M. In-situ X-ray Reflectivity Study of Incipient Oxidation of Pt(111) Surface in Electrolyte Solutions. *J. Chem. Phys.* **1994**, *100*, 4699.

(14) You, H.; Nagy, Z. Oxidation-reduction-induced Roughening of Platinum (111) Surface. *Phys. B* **1994**, *198*, 187−194.

(15) Nagy, Z.; You, H. Applications of Surface X-ray Scattering to Electrochemistry Problems. *Electrochim. Acta* **2002**, *47*, 3037−3055.

(16) Liu, Y.; Barbour, A.; Komanicky, V.; You, H. X-ray Crystal Truncation Rod Studies of Surface Oxidation and Reduction on Pt(111). *J. Phys. Chem. C* **2016**, *120*, 16174−16178.

(17) Goryachev, A.; Carlà, F.; Drnec, J.; Onderwaater, W. G.; Felici, R.; Krause, P. P.; Wonders, A. H.; Hensen, E. J.; Hofmann, J. P. Synchrotron Based Operando Surface X-ray Scattering Study

Towards Structure−activity Relationships of Model Electrocatalysts. *ChemistrySelect* **2016**, *1*, 1104−1108.
(18) Drnec, J.; Ruge, M.; Reikowski, F.; Rahn, B.; Carlà, F.; Felici, R.; Stettner, J.; Magnussen, O. M.; Harrington, D. A. Initial Stages of Pt(111) Electrooxidation: Dynamic and Structural Studies by Surface X-ray Diffraction. *Electrochim. Acta* **2017**, *224*, 220−227.
(19) Ruge, M.; Drnec, J.; Rahn, B.; Reikowski, F.; Harrington, D. A.; Carlà, F.; Felici, R.; Stettner, J.; Magnussen, O. M. Structural Reorganisation of Pt(111) Electrodes by Electrochemical Oxidation and Reduction. *J. Am. Chem. Soc.* **2017**, *139*, 4532−4539.
(20) Ruge, M.; Drnec, J.; Rahn, B.; Reikowski, F.; Harrington, D. A.; Carlà, F.; Felici, R.; Stettner, J.; Magnussen, O. M. Electrochemical Oxidation of Smooth and Nanoscale Rough Pt(111): An In Situ Surface X-ray Scattering Study. *J. Electrochem. Soc.* **2017**, *164*, H608−H614.
(21) Sugawara, S.; Itaya, K. In Situ Scanning Tunnelling Microscopy of a Platinum {111} Surface in Aqueous Sulphuric Acid Solution. *J. Chem. Soc., Faraday Trans. 1* **1989**, *85*, 1351.
(22) Itaya, K. In Situ Scanning Tunneling Microscopy of Platinum (111) Surface with the Observation of Monatomic Steps. *J. Vac. Sci. Technol. A Vacuum, Surfaces, Film* **1990**, *8*, 515.
(23) Sashikata, K.; Furuya, N.; Itaya, K. In Situ Electrochemical Scanning Tunneling Microscopy of Single-crystal Surfaces of Pt(111), Rh(111), and Pd(111) in Aqueous Sulfuric Acid Solution. *J. Vac. Sci. Technol., B: Microelectron. Process. Phenom.* **1991**, *9*, 457.
(24) Breuer, N.; Funtikov, A.; Stimming, U.; Vogel, R. In Situ Electrochemical STM Imaging of Roughened Gold and Platinum Electrode Surfaces. *Surf. Sci.* **1995**, *335*, 145−154.
(25) Furuya, N.; Shibata, M. Structural Changes at Various Pt Single Crystal Surfaces with Potential Cycles in Acidic and Alkaline Solutions. *J. Electroanal. Chem.* **1999**, *467*, 85−91.
(26) Löffler, T.; Bussar, R.; Xiao, X.; Ernst, S.; Baltruschat, H. The Adsorption of Ethene on Vicinally Stepped Electrode Surfaces and the Effect of Temperature. *J. Electroanal. Chem.* **2009**, *629*, 1−14.
(27) Wakisaka, M.; Asizawa, S.; Uchida, H.; Watanabe, M. In Situ STM Observation of Morphological Changes of the Pt(111) Electrode Surface During Potential Cycling in 10 mM HF Solution. *Phys. Chem. Chem. Phys.* **2010**, *12*, 4184−4190.
(28) Drnec, J.; Harrington, D. A.; Magnussen, O. M. Electro-oxidation of Pt(111) in Acid Solution. *Current Opinion in Electrochemistry* **2017**, *4*, 69−75.
(29) Jacobse, L.; Huang, Y. F.; Koper, M. T. M.; Rost, M. J. Correlation of Surface Site Formation to Nanoisland Growth in the Electrochemical Roughening of Pt(111). *Nat. Mater.* **2018**, *17*, 277−282.
(30) Yanson, Y. I.; Rost, M. J. Structural Accelerating Effect of Chloride on Copper Electrodeposition. *Angew. Chem., Int. Ed.* **2013**, *52*, 2454−2458.
(31) Yanson, Y. I.; Schenkel, F.; Rost, M. J. Design of a High-speed Electrochemical Scanning Tunneling Microscope. *Rev. Sci. Instrum.* **2013**, *84*, 023702.
(32) Rost, M. J. High-Speed Electrochemical STM. In *Encyclopedia of Interfacial Chemistry: Surface Science and Electrochemistry*; Wandelt, K., Ed.; Elsevier, 2018; Vol. *1*, pp 180−198.
(33) Solla-Gullón, J.; Rodríguez, P.; Herrero, E.; Aldaz, A.; Feliu, J. M. Surface Characterization of Platinum Electrodes. *Phys. Chem. Chem. Phys.* **2008**, *10*, 1359−1373.
(34) Vidal-Iglesias, F. J.; Arán-Ais, R. M.; Solla-Gullón, J.; Herrero, E.; Feliu, J. M. Electrochemical Characterization of Shape-controlled Pt Nanoparticles in Different Supporting Electrolytes. *ACS Catal.* **2012**, *2*, 901−910.
(35) McCrum, I. T.; Janik, M. J. Deconvoluting Cyclic Voltammograms To Accurately Calculate Pt Electrochemically Active Surface Area. *J. Phys. Chem. C* **2017**, *121*, 6237−6245.
(36) Arán-Ais, R. M.; Solla-Gullón, J.; Herrero, E.; Feliu, J. M. On the Quality and Stability of Preferentially Oriented (100) Pt Nanoparticles: An Electrochemical Insight. *J. Electroanal. Chem.* **2018**, *808*, 433−438.
(37) García-Aráez, N.; Climent, V.; Feliu, J. M. Potential-dependent Water Orientation on Pt(1 1 1) Stepped Surfaces from Laser-pulsed Experiments. *Electrochim. Acta* **2009**, *54*, 966−977.
(38) Furuya, N.; Koide, S. Hydrogen Adsorption on Platinum Single-crystal Surfaces. *Surf. Sci.* **1989**, *220*, 18−28.
(39) Domke, K.; Herrero, E.; Rodes, A.; Feliu, J. M. Determination of the Potentials of Zero Total Charge of Pt(100) Stepped Surfaces in the [011] zone. Effect of the Step Density and Anion Adsorption. *J. Electroanal. Chem.* **2003**, *552*, 115−128.
(40) Gómez, R.; Clavilier, J. Electrochemical Behaviour of Platinum Surfaces Containing (110) Sites and the Problem of the Third Oxidation Peak. *J. Electroanal. Chem.* **1993**, *354*, 189−208.
(41) Diaz-Morales, O.; Hersbach, T. J. P.; Badan, C.; Garcia, A. C.; Koper, M. T. M. Hydrogen Adsorption on Nano-structured Platinum Electrodes. *Faraday Discuss.* **2018**, *210*, 301−315.
(42) Sekerka, R. F. Equilibrium and Growth Shapes of Crystals: How Do They Differ and Why Should We Care? *Cryst. Res. Technol.* **2005**, *40*, 291−306.
(43) Schulze Icking-Konert, G.; Giesen, M.; Ibach, H. Novel Method for the Experimental Determination of Step Energies. *Phys. Rev. Lett.* **1999**, *83*, 3880−3883.
(44) Attard, G. A.; Harris, C.; Herrero, E.; Feliu, J. The Influence of Anions and Kink Structure on the Enantioselective Electro-oxidation of Glucose. *Faraday Discuss.* **2002**, *121*, 253−266.
(45) Clavilier, J.; Orts, J.; Gómez, R.; Feliu, J.; Aldaz, A. Comparison of Electrosorption at Activated Polycrystalline and Pt(531) Kinked Platinum Electrodes: Surface Voltammetry and Charge Displacement on Potentiostatic CO Adsorption. *J. Electroanal. Chem.* **1996**, *404*, 281−289.
(46) Note that, strictly speaking, step roughening occurs already at all temperatures above 0 K, as there is always enough entropy to place a kink into a step: one only has to increase the step lengths.[57]
(47) Björling, A.; Feliu, J. M. Electrochemical Surface Reordering of Pt(111): A Quantification of the Place-exchange Process. *J. Electroanal. Chem.* **2011**, *662*, 17−24.
(48) McCrum, I. T.; Hickner, M. A.; Janik, M. J. First-Principles Calculation of Pt Surface Energies in an Electrochemical Environment: Thermodynamic Driving Forces for Surface Faceting and Nanoparticle Reconstruction. *Langmuir* **2017**, *33*, 7043−7052.
(49) Topalov, A. A.; Katsounaros, I.; Auinger, M.; Cherevko, S.; Meier, J. C.; Klemm, S. O.; Mayrhofer, K. J. J. Dissolution of Platinum: Limits for the Deployment of Electrochemical Energy Conversion? *Angew. Chem., Int. Ed.* **2012**, *51*, 12613−12615.
(50) Lopes, P. P.; Strmcnik, D.; Tripkovic, D.; Connell, J. G.; Stamenkovic, V. R.; Markovic, N. M. Relationships between Atomic Level Surface Structure and Stability/Activity of Platinum Surface Atoms in Aqueous Environments. *ACS Catal.* **2016**, *6*, 2536−2544.
(51) Sugawara, Y.; Sasaki, M.; Muto, I.; Hara, N. Dissolution of Platinum Single Crystal Surfaces under Potential Cycling in Sulfuric Acid Solution. *ECS Trans.* **2014**, *64*, 81−87.
(52) Rost, M. J.; Jacobse, L.; Koper, M. T. M. The Dualism between Adatom- and Vacancy-based Single Crystal Growth Models. *Nat. Commun.* **2019**, in press. DOI: 10.1038/s41467-019-13188-0.
(53) Bott, M.; Hohage, M.; Michely, T.; Comsa, G. Pt(111) Reconstruction Induced by Enhanced Pt Gas-phase Chemical Potential. *Phys. Rev. Lett.* **1993**, *70*, 1489−1492.
(54) Hohage, M.; Michely, T.; Comsa, G. Pt(111) Network Reconstruction: Structure, Growth and Decay. *Surf. Sci.* **1995**, *337*, 249−267.
(55) Michely, T.; Hohage, M.; Esch, S.; Comsa, G. The Effect of Surface Reconstruction on the Growth Mode in Homoepitaxy. *Surf. Sci.* **1996**, *349*, L89−L94.
(56) Wang, S. C.; Ehrlich, G. Structure, Stability, and Surface Diffusion of Clusters: Irx on Ir(111). *Surf. Sci.* **1990**, *239*, 301−332.
(57) Ibach, H. *Physics of Surfaces and Interfaces*; Springer, 2006; Vol. *2006*; p 646.
(58) Walter, A. L.; Schiller, F.; Corso, M.; Merte, L. R.; Bertram, F.; Lobo-Checa, J.; Shipilin, M.; Gustafson, J.; Lundgren, E.; Brión-Ríos, A. X.; Cabrera-Sanfelix, P.; Sánchez-Portal, D.; Ortega, J. E. X-ray

DOI: 10.1021/acscentsci.9b00782
ACS Cent. Sci. 2019, 5, 1920−1928

Photoemission Analysis of Clean and Carbon Monoxide-chemisorbed Pt(111) Stepped Surfaces Using a Curved crystal. *Nat. Commun.* **2015**, *6*, 8903.
(59) Clavilier, J.; Armand, D.; Sun, S.; Petit, M. Electrochemical Adsorption Behaviour of Platinum Stepped Surfaces in Sulphuric Acid Solutions. *J. Electroanal. Chem. Interfacial Electrochem.* **1986**, *205*, 267−277.
(60) McCrum, I. T.; Janik, M. J. pH and Alkali Cation Effects on the Pt Cyclic Voltammogram Explained Using Density Functional Theory. *J. Phys. Chem. C* **2016**, *120*, 457−471.
(61) Chen, X.; McCrum, I. T.; Schwarz, K. A.; Janik, M. J.; Koper, M. T. Co-adsorption of Cations as the Cause of the Apparent pH Dependence of Hydrogen Adsorption on a Stepped Platinum Single-Crystal Electrode. *Angew. Chem., Int. Ed.* **2017**, *56*, 15025−15029.
(62) Van Der Niet, M. J.; Garcia-Araez, N.; Hernández, J.; Feliu, J. M.; Koper, M. T. Water Dissociation on Well-defined Platinum Surfaces: The Electrochemical Perspective. *Catal. Today* **2013**, *202*, 105−113.

DOI: 10.1021/acscentsci.9b00782
ACS Cent. Sci. 2019, 5, 1920−1928